

# Automated Structural-level Alignment of Multi-view TLS and ALS Point Clouds in Forestry

Juan Castorena<sup>a</sup>, L. Turin Dickman<sup>a</sup>, Adam J. Killebrew<sup>a</sup>, James R Gattiker<sup>a</sup>, Rod Linn<sup>a</sup>, E. Louise Loudermilk<sup>b</sup>

<sup>a</sup>Los Alamos National Laboratory, Los Alamos, NM, 48124 USA

<sup>b</sup>Southern Research Station, 200 W.T. Weaver Blvd. Asheville, NC 28804-3454, USA

---

## Abstract

Access to highly detailed models of heterogeneous forests from the near surface to above the tree canopy at varying scales is of increasing demand as it enables more advanced computational tools for analysis, planning, and ecosystem management. LiDAR sensors available through different scanning platforms including terrestrial, mobile and aerial have become established as one of the primary technologies for forest mapping due to their inherited capability to collect direct, precise and rapid 3D information of a scene. However, their scalability to large forest areas is highly dependent upon use of effective and efficient methods of co-registration of multiple scan sources. Surprisingly, work in forestry in GPS denied areas has mostly resorted to methods of co-registration that use reference based targets (e.g., reflective, marked trees), a process far from scalable in practice. In this work, we propose an effective, targetless and fully automatic method based on an incremental co-registration strategy matching and grouping points according to levels of structural complexity. Empirical evidence shows the method's effectiveness in aligning both TLS-to-TLS and TLS-to-ALS scans under a variety of ecosystem conditions including pre/post fire treatment effects, of interest to forest inventory surveyors.

*Keywords:* Registration, LiDAR, Point Cloud, ALS, TLS, Automatic, Forest, Targetless

---

## 1. Introduction

Forests cover approximately four billion hectares amounting to roughly 31% of the earth's land area [1]. Demand for tools that help maintain the balance of a healthy forest ecosystem are increasing but their complexity is challenging as it depends on a wide range of factors including resilience against disease and fire, health and biodiversity [2]. Methods that help collect information about these factors and that consider the heterogeneity of the forest and its changes over time is an active area of research seeking to provide the means for improved planning, management, analysis and more effective and efficient decision-making [3]. Traditionally, one of the most widely used tools for measurement are national forest inventory (NFI) plots that use spatial sampling and estimation techniques to quantify factors including forest cover, growing stock volume, biomass, carbon balance and tree measurements (e.g., diameter at breast height, crown width, height) [4]. Limitations are however, that these plots are typically field sampled by hand, which can be economically costly and time consuming especially when considering large spatial scales extents (e.g., 1 million ha).

Remote sensing techniques including terrestrial laser scanning (TLS), aerial laser scanning (ALS) and optical photogrammetry have been established as technologies offering time and cost economies at scale [2] in forest surveys. From these, LiDAR based scanning has gained widespread interest due to its inherent capabilities to directly collect precise 3D structural information very rapidly and over large regional extents [5]. Airborne based LiDAR for example, utilizing accurate position sensors including RTK, enables large scale mapping at spatial resolutions in the order of  $\sim 10$  pts/m<sup>2</sup>. It has shown to be effective in retrieving factors of interest in forest inventory plots [6], however, some limitations exist as it has problems penetrating the tree canopy cover in dense areas even with its powerful but computationally demanding full-waveform based technology. TLS, on the other hand [7], is complementary to ALS as it is capable of collecting 3D maps at much higher spatial resolutions providing detailed 3D information about individual trees, shrubs, ground surface and near ground vegetation. However, strategies and methods for moving the scanning system and fusing their data from multiple scans to increase the field of view can be challenging. The

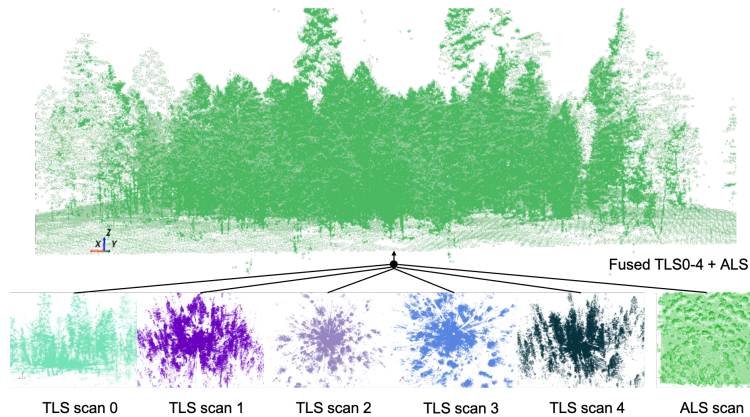


Figure 1: Alignment of 5 multi-view TLS and ALS in New Mexico forest.

simplest of strategies consists of placing the scanner at different locations within a plot (i.e., multi-view TLS), but other more sophisticated options exist including hand-held scanners [8]. Having access to a diversity of sources can offer the enhanced capabilities of all: enabling precise, 3D information from the near surface vegetation to the top of the canopy at scale; a characteristic rarely available when a single scanning mode is used [7]. Here, we focus our scope on one of the fundamental enablers for combining scanning sources in forest ecosystems: co-registration or alignment approaches allowing projection of multi-source data into a common, consistent coordinate system.

Most studies that establish the complementary nature between multi-view TLS and ALS in forestry [9, 8, 10, 11, 12] have utilized known physically placed reference targets (e.g., multiple uniform size spheres, retro-reflective targets), which are detected and matched between scans for alignment. Unfortunately, this group of target based methods tends to render LiDAR data collection less scalable and more time consuming. In contrast, targetless methods in forestry [13, 14, 15, 16, 17, 18] have used extracted tree features (e.g., stem size, stem axis, breast height, distances between trees) for finding alignment correspondences. These methods tend, however, to be sensitive to the accuracy of the tree extraction method; a process that can become computationally demanding in dense forest areas and prone to significant errors. Other alternatives have resorted to position sensors including GNSS/IMU systems in multi-view TLS in forestry settings [8], but have found inferior performances due to higher uncertainties or missing measurements in areas of poor or nonexistent satellite based georeferencing [19].

Within the fields of computer vision and robotics, many automatic and targetless point cloud registration methods exist. Examples include the seminal iterative closest point (ICP) [20], point-to-plane ICP [21], 4 point co-planar sets [22], feature point feature histograms (FPFH) [23] and more recent learning based co-registration methods [24, 25]. These methods do not require a target and use rule or learned based features within the scene to find correspondences. Applications involving point clouds from shaped objects and urban scenes have been very successful for registration using these approaches. However, such methods typically assume a highly structured environment and suffer when applied in a straightforward manner in complex heterogeneous forest ecosystems. The presence of non-uniform structures such as bushes, leaves, bark, branches on the forest surface, dense and heterogeneous tree types, and the non-uniformity of the forest surface can make standard registration methods highly prone to miss-alignment. This conclusion applies also to more sophisticated deep learning based methods [26]. In addition, partial (i.e., existing only in a limited region), as opposed to sparse or full overlap, is also problematic for most conventional 3D registration approaches. This is often the case in forests, where both sensor ranges and distances between scan centers and occlusion in densely populated forests from vegetation or steep terrain may have a significant effect. In the more specific case of TLS-to-TLS co-registration, several works have been proposed. In urban scenarios for example, the work of [27] approximated scenes by planar patches and used them as features to globally optimize the alignment parameters. [28] projected 3D points into a ground occupancy 2D plane image and based its registration approach in aligning these occupancy planes. Along a similar principle, [29] proposed a bird's eye view 3D-to-2D point cloud projection method and used SIFT features to register scan pairs. These set of methods however, were designed to register highly structured urban environments containing buildings, houses and man-made structures and do not work

well in cases where the scene does not contain sharp edges, corners or planar like shapes. TLS-to-TLS methods operating in forestry environments includes the recent work of [30] specifically focused on registering TLS scans. It relies on semantic segmentation of tree stem and branch centers of scans but is restricted to single tree scans. On the other hand, [31] used the starting points of tree LiDAR shadows (i.e., vertex of cone shaped projection areas without LiDAR returns caused by tree occlusion) as features to co-register adjacent TLS scans. Accuracies at the level of target based methods were achieved, but the evaluation performed in the study was limited to only 17 scan pairs. Other recent TLS methods rely on finding correspondances between extracted tree attributes (e.g., stems [14, 15, 16, 32], tree locations [33]). Their accuracies are highly dependent on the performance of semantic segmentation of tree attributes and is thus prone to co-registration errors in cases of low semantic segmentation performance which commonly occurs in high tree density forests. On the TLS-to-ALS side, most works rely on using features suitable to urban scenarios and are thus not applicable to natural forest environments. The work of [34] for example, used wavelets to detect edges in buildings and later matched these in between TLS and ALS for registration. [35] instead registered scans by extracting and matching planar like structures while [36] used both edges and planes to register scans containing buildings. The works of [37, 38, 39] extracts urban building outlines/contours/boundaries and is thus dependent on the regularity of corners, edges and planes for this purpose. But as in all the aforementioned methods, these works focus on registering urban scenes and their fundamental step of feature extraction/correspondence is not suitable for forest ecosystems. Recent efforts in [16, 17, 33, 32, 40] proposed methods to register LiDAR scans coming from forest environments by finding relative tree attributes. For example, [41, 17] finds correspondances between ALS and TLS through tree position extractions. Correspondance and alignment of tree crown features are used in [42, 43]. Alignments from relative tree-heights between scan sources are exploited in [44]. The efficacy of these methods however, is dependent upon the accuracy of the tree segmentation step which tends to degrade as a function of increasing tree density while also becoming increasingly time consuming. Methods using manually placed reference targets do not apply in the TLS-to-ALS setting due to practical challenges including finding targets visible to both sources, and time disparities between TLS and ALS data collection surveys.

In light of these limitations, we propose a new automatic and targetless co-registration method based on a notion of structural complexity; used as a similarity metric encoding information about LiDAR point distribution. We show, grouping and matching scan point subsets based on structural complexity is an effective strategy for finding groups of point correspondances and co-registering pairs of scans from highly complex and heterogeneous forest environments under a variety of conditions. Figure 1 illustrates an example result for the refined alignment of five color-coded multi-view TLS scans from a New Mexico, USA forest. Advantages of the proposed method are its effectiveness in registering LiDAR scans in complex forest environments, while not requiring position sensors, reference human placed targets, extraction of trees or other semantic features, and being fully automatic. Section 2 describes our approach more in detail while Section 3 shows the overall performance of our method along with a few illustrative examples. Finally, Section 4 includes a short discussion about the benefits of the proposed method to applications in forest studies and Section 5 summarizes our contributions and findings.

## 2. Approach

Co-registration of multiple LiDAR point cloud sources seeks to align and stitch/accumulate all scan sources into a global or common and consistent coordinate system. Scan sources can come from multi-view perspectives, different sensors, scanning platforms (e.g., static TLS, mobile TLS, UAV’s, ALS). As we are focusing on methods that are both automatic, targetless and without the use of position and orientation sensing, we restrict our approach to scan sources that have at least partial field of view (FOV) overlap. This section describes the proposed alignment method mainly consisting of two stages: (1) an incremental multi-structural complexity co-registration of scan pairs and (2) a bundle refinement distributing errors between multiple overlapping scan views. To the best of our knowledge, this is the first fully automatic and targetless based method capable of co-registering both TLS-to-TLS and TLS-to-ALS scans under a variety of forest ecosystem conditions and that does not depend on the accuracy of any prior semantic segmentation approach (e.g., tree detection and segmentation).

In terms of notation, a LiDAR scan is denoted by  $\mathbf{X} \in \mathbf{R}^{N \times 3}$  with  $N$  being the number of points in the scan and 3 being the point coordinates in the  $x, y$  and  $z$ -axes. A subscript  $s$  or  $t$  attached to the right of a scan as  $\mathbf{X}_s$  is used to distinguish between a source  $s$  and a target  $t$  scan while a superscript  $i$  as in  $\mathbf{X}^{(i)}$  denotes a selection of point(s) according to index or index set  $i$ . For a pair of scans, registration is characterized by an aligning rigid body

transformation consisting of 6 orientation/position degrees of freedom (DOF): three rotation angles ( $\theta_{\text{roll}}, \theta_{\text{pitch}}, \theta_{\text{yaw}}$ ) and three translations ( $t_x, t_y, t_z$ ). 3D rotations are represented by the matrix  $\mathbf{R} \in \mathbf{SO}(3)$  in the special orthogonal group  $\mathbf{SO}(3)$  while translations are equivalently denoted as the vector  $\mathbf{t} \in \mathbb{R}^3$  of  $t_x, t_y, t_z$  coordinate elements. The subscript and superscripts attached on the right of  $\mathbf{R}, \mathbf{t}$  denotes that this transformation takes from the coordinate system of the subscript, to that of the superscript while the subscript  $m$  attached to the left of  $\mathbf{R}, \mathbf{t}$  denotes the  $m$ -th index.

### 2.1. Pair-wise co-registration

The core idea of the proposed pair-wise registration approach is to align pairs of scans by incrementally aligning matching groups of scan point subsets grouped and matched by structural complexity similarities. Rather than using standard human engineered or learned features, we make use of a notion of structural complexity to establish similarity. This, different from standard methods relying on features characteristic of human made objects or scenes (e.g., corners, edges, planar facets, contours, spheres, etc.) which rarely appear in complex heterogeneous forests, or from semantic segmentation-based methods (e.g., tree attributes) relying on accurate estimates. The main ingredients of our co-registration approach include: (1) the similarity metrics to establish scan point group correspondance, (2) grouping and matching which entails associating scan point subsets according to their structural similarities and, (3) the optimization strategy of the co-registration parameters from the matched groups of scan points. In the following, we include the mathematical descriptions and steps encompassing each of these.

#### 2.1.1. Similarity metrics

Structural complexity (SC) here, is a metric encoding information uncertainty in point range distributions at relative height point-to-plane projections. Structural similarities (SS) on the other hand are computed by uncertainty in conditional point range distributions. These metrics are meant as a quick method for comparisons, group and match sets of points as they only involve low-level operations without the need of any semantics. The mathematical descriptions of structural complexity (SC) and similarity (SS) utilized here are based on entropy and mutual information (MI) [45] measures from information theory. Here, SC is measured by:

$$\text{SC}(q, k) = \sum_{\text{span}(r)} p\left(r(\mathbf{X}_q^{(j_q^k)})\right) \log p\left(r(\mathbf{X}_q^{(j_q^k)})\right) \quad (1)$$

where  $p$  is a probability distribution of point ranges relative to the point-to-plane projection indexed by  $(q, k)$  defined over the span of ranges  $\text{span}(r)$  (e.g., from 0-50 m at uniform 0.25 m steps),  $r : \mathbb{R}^{N \times 3} \rightarrow \mathbb{R}^{+N \times 1}$  is a function computing the range of point-to-plane projections and the index set  $j_q^k$  is formed by the union of scan points bounded a distance  $\Delta z$  away from the plane indexed by  $(q, k)$ . SS computes structural similarities between pairs of points  $\mathbf{X}_s^{(i^s)}$  and  $\mathbf{X}_t^{(i^t)}$  grouped and indexed by  $i^a$ . These groups are now formed by point indices  $i^a$  joined according to structural complexity and extracted independently for each source and target scans. Mathematically SS is described as:

$$\text{SS}(\mathbf{X}_s^{(i^s)}, \mathbf{X}_t^{(i^t)}) = \sum_{\text{span}(r)} \sum_{\text{span}(r)} p\left(r(\mathbf{X}_s^{(i^s)}), r(\mathbf{X}_t^{(i^t)})\right) \log \frac{p\left(r(\mathbf{X}_s^{(i^s)}), r(\mathbf{X}_t^{(i^t)})\right)}{p\left(r(\mathbf{X}_s^{(i^s)})\right) p\left(r(\mathbf{X}_t^{(i^t)})\right)}. \quad (2)$$

The principle behind Eq.(2) is similar to MI which has been shown to be effective in registering multiple sensing modalities [46] as an optimization metric, but here we use it only to group and match point subsets intra/inter-scan. Similarly, point-to-plane projections have been used before for registering LiDAR scans as a feature compression mechanism. Here, however, we do not use projected points as features for registration as in [37, 38, 28, 39, 29], but rather for grouping points and finding correspondences between groups. Also, the sliding point-to-plane projection strategy is different from previous works that only use a single bird's eye view as features [37, 38]. Furthermore, notions of structural scene complexity have been used previously in [47, 48], but therein used to sub-sample scenes at varying complexity based on the waveform envelope shapes in full-waveform LiDAR.

#### 2.1.2. Grouping and Matching

Grouping and matching is an algorithm developed here to group and match point subsets by structural similarity. It encompasses two tasks: (1) Intra-scan groupings, conglomerating point subsets of a scan into levels of structural

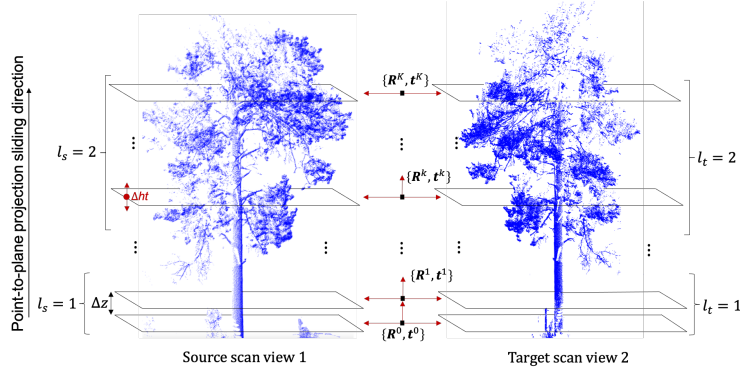


Figure 2: Multilevel registration of example scans.

similarity and (2) Inter-scan matching, encompassing matching structurally similar levels between pairs of source and target scans. Intra-scan point group subsets are formed by sequentially sliding a plane in the direction of a plane’s normal and associating in a set of indices  $j_q^k$  for sliding plane index  $k \in \{1, \dots, K\}$  and scan  $q \in \{s, t\}$  points which are at most a normal distance  $\Delta ht$  away. The sliding plane starts at the ground of the scan (i.e.,  $k = 0$ ) and moved up at uniform shifts  $\Delta z$  until  $K$ . An illustration of this is included in Figure 2 showing a tree from a source and a target scan view. The range of each point in the  $x, y$  direction relative to the plane’s axis center is then computed through a point-to-plane projection further used to obtain a histogram representing point range distribution. Point range distributions across sliding planes parametrized by plane parameters  $\phi$  at height  $k\Delta z$  are compared to find structural similarities between them and those found similar are organized into groups each representing a complexity level. Here, we make use the simple  $k$ -means algorithm [49] to determine the intra-levels which are similar based on their complexity. The number of groups representing complexity can vary depending on the scene but throughout all experiments here we set this to three (i.e., in the  $k$ -means algorithm) for each scan. The reference plane at  $k = 0$  is extracted by fitting the closest 3D plane with the random sampling and consensus (RANSAC) algorithm [50].

Inter-scan matching seeks to find correspondences in structural complexity levels between the scans. Matchings are posed as an assignment problem with a one-to-one correspondence between the formed scan point groups in the source and target scans. This is formulated as the bijective matching that maximizes the sum of pair-wise SS’s:

$$\hat{\mathbf{A}} = \arg \max \sum_{l_s} \sum_{l_t} A_{l_s, l_t} \text{SS}(\mathbf{X}_s^{(l_s)}, \mathbf{X}_t^{(l_t)}) \quad (3)$$

subject to the constraints that  $A_{l_s, l_t} \in \{0, 1\}$  and  $\sum_{l_s} A_{l_s, l_t} = 1, \sum_{l_t} A_{l_s, l_t} = 1, \forall l_s, l_t$ . Eq.(3) thus finds the optimal correspondance between scan group sources with SS computed via Eq.(2). Similar problems has been formulated before in the context of computing 3D LiDAR point flows in [51] but here to match structural level similarities between scans. Solutions to this problem exist in [52]. For compactness, we represent the estimate  $\hat{\mathbf{A}}$  through the matched indices function between source levels  $l_s \in \{1, \dots, L\}$  and target level  $l_t \in \{1, \dots, L\}$  as  $l_t = \sigma(l_s)$  where the support of  $\sigma : \mathbb{Z} \rightarrow \mathbb{Z}$  is denoted as  $L = |\sigma|$ .

### 2.1.3. Alignment Optimization

The proposed co-registration approach employs an incremental optimization strategy that provides the capability to improve alignment estimates over time and inherits its ability to recover from bad initial or first iterate estimates. The grouped scan points obtained as described in Section 2.1.2 are co-registered per matched groups with an incremental strategy starting from the corresponding levels of lower structural complexity (e.g.,  $l = 0$ ) and moving up into the more complex with complexities measured as in Eq.(1) using the point indices of  $i_s^l$ . At each matched structural level ICP is used as optimization only at the points indexed by  $i_s^l$  and the matched  $i_t^{\sigma(l_s)} = i_t^l$  for the specific level  $l_s$ . The resulting transformation  $\{\mathbf{R}^l, \mathbf{t}^l\}$  is subsequently used as initialization at the next complexity level and so forth, thus its incremental nature, until a pre-defined level  $L$  is reached (e.g.,  $L=3$  as used in all experiments here). One thing to note here is that the indexed point cloud at each structural level is downsampled (denoted as a  $\downarrow_{\delta_s}$  attached next to a

---

**Algorithm 1** Pair-wise multi-structural level co-registration
 

---

```

1: Input: Source  $\mathbf{X}_s$  and target  $\mathbf{X}_t$  point clouds.
2: Set: downsampling factors  $\delta_0 = 0.25(\text{m})$ ,  $\delta = 0.025(\text{m})$ ,  $\Delta ht = 0.25(\text{m})$ , plane shifts  $K = \frac{\max \text{ height}}{\Delta ht}$ , structural groups  $L = 3$ 
3:   Initializations  $\mathbf{R}^0 = \mathbf{I}_{3 \times 3}$  (identity),  $\mathbf{t}^0 = \mathbf{0}_{3 \times 1}$  (zero vector).
4: Intra-scan groupings:
5:   for  $q$  in  $\{s, t\}$  do:
6:     Downsample point clouds  $\tilde{\mathbf{X}}_q = \mathbf{X}_q \downarrow_{\delta_0}$ 
7:     Get most dominant plane  $\phi_q = \text{RANSAC}\{\tilde{\mathbf{X}}_q\}$ 
8:     for  $k$  in  $[0, \dots, K]$  do:
9:       // Extract points bounded a distance away from point-to-plane projection
10:       $J_q^k = \{i : \phi_q \tilde{\mathbf{X}}_q^i \geq (k-1) \cdot \Delta ht \ \& \ \phi_q \tilde{\mathbf{X}}_q^i < k \cdot \Delta ht \ \forall i\}$ 
11:    end
12:    // Group point indices by structural similarities using  $k$ -means.
13:     $\ell_q = k\text{-means}([\text{SC}(q, 0), \text{SC}(q, 1), \dots, \text{SC}(q, K)], L)$  with  $\ell_q = \cup_{l=1}^L \ell_q^l = \{0, 1, \dots, K\}$ 
14:     $I_q^l = \{J_q^k : k \in \ell_q^l\}$ 
15:  end
16:  Output: Structural complexity scan point level indices  $\{I_s^l, I_t^l\}$ 
17: Inter-scan level matchings:
18:  Use  $\text{SS}(\mathbf{X}_s^{I_s^l}, \mathbf{X}_t^{I_t^l})$  in Eq. (3) and compute  $\sigma$  with  $L = |\sigma|$ 
19: Incremental registration:
20:  for  $l$  in  $[1, \dots, L]$  do:
21:     $\{\mathbf{R}^l, \mathbf{t}^l\} = \text{ICP}(\tilde{\mathbf{X}}_s^{I_s^l}, \tilde{\mathbf{X}}_t^{I_t^l}, \{\mathbf{R}^{l-1}, \mathbf{t}^{l-1}\})$ 
22:  end
23:  run:  $\{\mathbf{R}, \mathbf{t}\} = \text{ICP}(\mathbf{X}_s \downarrow_{\delta}, \mathbf{X}_t \downarrow_{\delta}, \{\mathbf{R}^L, \mathbf{t}^L\})$ 
24: Output: Rotation and translation  $\{\mathbf{R}, \mathbf{t}\}$ .

```

---

scan  $\mathbf{X}$ ) using a uniform grid of cell size  $\delta_{I_s}$  to reduce differences in point densities between scans and to minimize the registration bias effect of areas that are more densely sampled due to proximity of objects to sensor (e.g., near surface in TLS or canopy in ALS). Moreover, this downsampling also reduces the computational demands of running ICP on densely sampled scan pairs. Here, we use the downsampling constant factor function with step size  $\delta_0 = 0.25$  (m.) throughout all levels, but others can be used depending on the scanning density characteristic of the sensor. In a last step, ICP is re-run on the entire point cloud using as initialization the last computed estimates  $\{\mathbf{R}^L, \mathbf{t}^L\}$  and just for a few iterates (e.g., 50) with a finer downsampling resolution (e.g.,  $\delta = 0.025$  (m.)). A summary of the whole described co-registration approach is included in Algorithm 1.

## 2.2. Bundle refinement

In bundle refinement, small errors resulting from pair-wise alignments are treated through bundle refinements to prevent error propagation in the presence of multiple pair-wise scans. This error is reduced by incorporating cycle consistency constraints between the multiple scans. The set of  $C$  scan sources are represented by a graph where each node is the center of each scan source  $\mathbf{c}_i$  for  $i \in \{0, \dots, C\}$  in the common/global coordinate system and edges are just artificial connections between any pair of nodes. The relative positions of scan node  $\mathbf{c}_1$  to  $\mathbf{c}_0$  connected by an edge can be expressed as in Eq.(4):

$$\mathbf{R}_{\mathbf{c}_1}^{\mathbf{c}_0} = \mathbf{R}_w^{\mathbf{c}_0} \mathbf{R}_{\mathbf{c}_1}^w, \quad \mathbf{t}_{\mathbf{c}_1}^{\mathbf{c}_0} = \mathbf{R}_w^{\mathbf{c}_0} (\mathbf{t}_{\mathbf{c}_0}^w - \mathbf{t}_{\mathbf{c}_1}^w) \quad (4)$$

where  $w$  represents a world coordinate system. Refinement is achieved by imposing a cycle consistency constraint between all paths connecting node  $\mathbf{c}_1$  to node  $\mathbf{c}_0$ . Here, a path in a graph is any sequence of edges connecting at least any two nodes. For ease of exposition Fig.3 illustrates this with a graph of five node scans. Non-exhaustive example paths between  $\mathbf{c}_1, \mathbf{c}_0$  in this case include:  $\mathbf{c}_1 \rightarrow \mathbf{c}_0$ ,  $\mathbf{c}_1 \rightarrow \mathbf{c}_2 \rightarrow \mathbf{c}_0$ ,  $\mathbf{c}_1 \rightarrow \mathbf{c}_3 \rightarrow \mathbf{c}_0$ ,  $\mathbf{c}_1 \rightarrow \mathbf{c}_4 \rightarrow \mathbf{c}_0$ ,  $\mathbf{c}_1 \rightarrow \mathbf{c}_3 \rightarrow \mathbf{c}_4 \rightarrow \mathbf{c}_2 \rightarrow \mathbf{c}_0$ . Similar to Eq.(4), the relative position between nodes  $c_i$  to  $c_j$  through a path  $m$  composed of  $N^m$  nodes indexed by  $n$  (abusing notation as  $n$  is assumed to respect the sequence order of nodes in the path), can

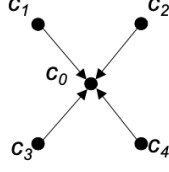


Figure 3: A graph with five nodes.

be obtained as in Eq.(5):

$${}_m\mathbf{R}_{\mathbf{c}_i}^{\mathbf{c}_j} = \prod_{n=i}^j \mathbf{R}_{\mathbf{c}_n}^{\mathbf{c}_{n+1}}, \quad {}_m\mathbf{t}_{\mathbf{c}_i}^{\mathbf{c}_j} = \sum_{n=i}^j \mathbf{t}_{\mathbf{c}_n}^{\mathbf{c}_{n+1}} \quad (5)$$

Here, the set of paths is of cardinality  $M$  and  $m$  is an index of a specific path. Imposing cycle consistency throughout all LiDAR scan sources thus consists in minimizing at each node  $\mathbf{c}_i$  the estimation errors from a set of paths. This can be formulated as the computation of the rotation and translation at  $\mathbf{c}_i$  that minimizes the sum of distances in Eq.(6):

$$\hat{\mathbf{R}}_{\mathbf{c}_i}^w = \arg \min_{\mathbf{R} \in \mathbf{SO}(3)} \left\{ \sum_{m=1}^M \|\log(\mathbf{R}^T {}_m\mathbf{R}_{\mathbf{c}_i}^w)\| \right\}, \quad \hat{\mathbf{t}}_{\mathbf{c}_i}^w = \arg \min_{\mathbf{t} \in \mathbb{R}^3} \left\{ \sum_{m=1}^M \|\mathbf{t}_{\mathbf{c}_i}^w - \mathbf{t}\|_{\ell_2} \right\} \quad (6)$$

where  $\|\log(\mathbf{R}^T {}_m\mathbf{R}_{\mathbf{c}_i}^w)\|$  is the Riemannian distance measuring the shortest geodesic between rotations and the second rotation term can be obtained as  ${}_m\mathbf{R}_{\mathbf{c}_i}^w = \mathbf{R}_{\mathbf{c}_j}^w \mathbf{R}_{\mathbf{c}_i}^{\mathbf{c}_j}$ . The intuition behind the problem in Eq.(6) is simple; in general, we find the rotation  $\mathbf{R} \in \mathbf{SO}(3)$  that minimizes the Euclidean distance between the vector of unit energy rotated by  $\mathbf{R}$  and a set of rotated sampled vector estimates each also of unit energy. Finding the parameters that optimally solve Eq.(6) relative to the rotations  $\mathbf{R}$  can be done using either the  $\ell_2$  average of rotations [53] computed by the exponential gradient descent or the more robust to outliers  $\ell_1$  average computed with the Weizfeld algorithm [54]. Solving Eq.(6) for the translation can be done by computing a  $\mathbf{t}$  at which the gradient of its cost is equal to zero which corresponds to the translation average.

### 3. Experiments

In the following set of experiments, we validate our approach in several case scenarios: pair-wise and multi-view registration. Validation is performed on real LiDAR point cloud datasets: (1) on multi-view TLS scans (2) on collocated TLS and ALS. Datasets were collected from a variety of forest ecosystems with most within the boundaries of the Bandelier National Monument in New Mexico, USA in high elevation mixed-conifer forest, unless otherwise specified. Implementations were performed in Python, with the VTK based PyVista module visualizer and using some tools from Open3d [55], in particular ICP and downsampling functionality.

#### 3.1. Datasets

The TLS dataset was collected in the summer of 2022 using a Leica BLK360 LiDAR with a laser scanner operating at a 830 nm wavelength and fields of view (FOV) of  $300^\circ$  and  $360^\circ$  in the vertical and horizontal directions, respectively. The LiDAR was mounted in a static tripod while scanning. The center locations of forest inventory plots (FIP) were used as reference for positioning a "center" LiDAR scan while multi-view scans were placed within the FIP quadrants that altogether define the FIP area coverage. A total of 21 plots were LiDAR surveyed and used each with five multi-view scans per plot. The inventory plots were 50 x 20 (m) and the LiDAR scans were positioned one at the center while the other four distributed  $\sim 15 \times 5$  meters apart from the center in each of the four corners similar to as shown in Fig. 3. An example of the distribution of points resulting from a single scan with a mostly flat ground surface is included in Figure 4.(a). Approximately 8 million points were measured per scan with 4.6 million reflected from the ground. Most of the returns are concentrated below the 15 (m) range in general, while most returns are below 10(m) for the ground surface.

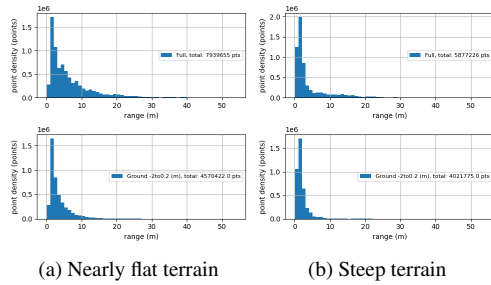


Figure 4: BLK360 LiDAR point cloud distribution.

The ALS data was collected in October 2021 by TetraTech over 170 square miles around Los Alamos, NM. The ALS system included a Galaxy T2000 LiDAR sensor mounted on a fixed-wing aircraft. The LiDAR operates with a 1064 nm wavelength laser and is capable of collecting up to 8 multiple returns per laser fired. The scan FOV of this LiDAR is 10-60° with an accuracy of <math><0.03-0.25\text{ m}</math> RMSE within the 150-6500 m range. The surveyed area was completed in 55 flight lines, including 7 cross strips to ensure a point density of 10 points per square meter. Note that the ALS datasets utilized here all include the 8 multiple returns per laser fired which increases the density of point returns from below the canopy. Since there is no occlusion for satellite signals in ALS, its scans were aligned with a Trimble CenterPoint RTX positioning system that delivers accuracies at the centimeter (cm) level.

*Performance Metrics:* All our quantitative evaluations were performed using the registration root mean square error (RMSE) metric. Here, registration RMSE was measured relative to the ground truth six degrees of freedom orientation and position registration parameters. Ground truth comes from different sources depending on the experiments performed. In Subsections 3.2.1-3.2.2 ground truth was obtained by running our approach on TLS ground scans for 10 trials on each pair-wise scan, averaging registration parameters and checking for consistency with augmented ALS. Consistency with ALS was verified by comparing with the relative orientations and positions found by localizing the TLS scan centers projected into the ground plane in ALS and finding the orientation and translations relative to each scan. Notice that RTX aligned ALS provides accuracies within the centimeter level. After these steps, the resulting registrations were validated by a trained expert. In Section 3.3.1 ground truth comes from a target reference based method from a LiDAR dataset collected in a Forest ecosystem. Evaluations were also benchmarked against other well known standard co-registration methods. Overlap is measured as % of points in source having at least a correspondence point in the target scan not exceeding 25 cms over the total number of points in the pair of scans. In the case of registration of multiple scans, overlap is measured similarly by counting the number of corresponding points in every pair-wise scan combination within a plot not exceeding 25 cms over the total number of points.

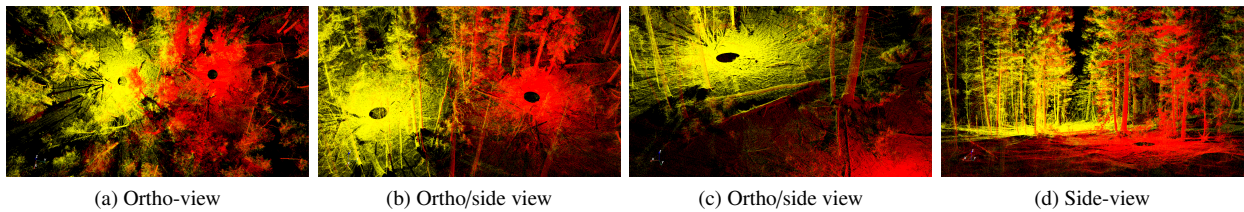


Figure 5: Pairwise alignment result of TLS based point clouds

### 3.2. Pair-wise TLS registration

#### 3.2.1. Overall results

The pair-wise registration method described in Section 2.1 was evaluated on pairs of multi-view TLS point clouds. Example results are shown in Fig. 5 illustrating four views of the registration of two color-coded scans 15 x 5 meters apart on a forest site including white fir, limber pine, aspen, and Douglas fir and surface bark, trunk and bushes. Fig. 5 shows well aligned point clouds and object consistency in between scan color transitions.



To test the overall performance of the proposed approach in a diverse set of forest conditions (including heterogeneous vegetation, gradient variations in topography) we performed pair-wise registrations in 21 distinct inventory plots for a total of 84 distinct pair scans. Each scan was originally in its ego-reference coordinate system and the registration approach was thus initialized to those ego-referenced parameters. Here, we refer to an ego-reference to measurements performed in the local "raw" sensor coordinate system. Each scan pair was physically separated by a translation distance of 15x5 m and a randomly oriented scan axis. The registration RMSE computed over all scan pairs including the plot center scan is summarized in Table 1. The results in this table show that the method is flexible and robust to operate under vegetation diversity and topography variations.

Table 1: Registration RMSE.

Orientation (Degrees)			Position (meters)		
$\theta_{\text{roll}}$	$\theta_{\text{pitch}}$	$\theta_{\text{yaw}}$	$t_x$	$t_y$	$t_z$
0.08	0.04	0.09	0.014	0.016	0.0011

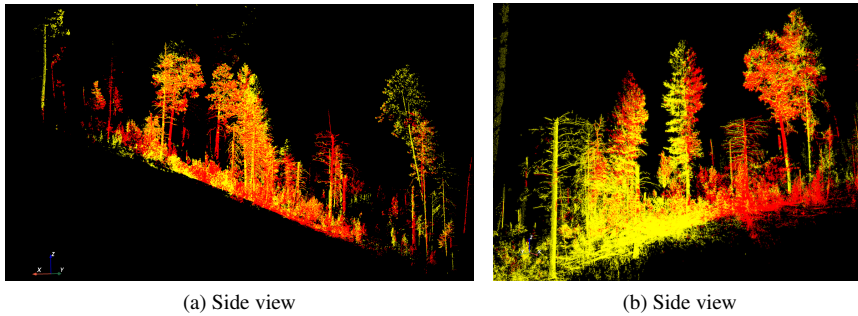


Figure 6: Pairwise TLS alignment in steep terrain.

### 3.2.2. Non-uniform ground terrain (forest gradient):

In forest environments there are challenging scenarios that could complicate registration. One example of these is the presence of steep ground terrain or *forest with gradient variations in topography*. The main issue with this complication is not from the gradient terrain itself but rather from the restricted field of view arising from this coupled with the nature of LiDAR scene scanning, potentially reducing the amount of overlap: a known cause for co-registration performance degradation. Figure 4.(a-b) which shows the distribution of points as a function of range illustrates this; the tails of the distribution in the more steep slope case are less heavy than in the nearly flat terrain. We include some additional experiments to test whether our multi-structural level approach was capable of registering under these more challenging case scenarios. Fig. 6.(a-b) gives two representative examples of the alignments produced by the proposed method with pairs of scans 10 m and 15 x 5 m apart, respectively. Both are from a plot including white fir, limber pine, aspen, Douglas fir, ponderosa pine trees. The method aligns the two-point clouds consistently throughout the entire scene despite the smaller overlap compared to the near flat terrain.

Table 2 summarizes experiments that evaluate registration performance as a function of % overlap. A total of 100 registration tests per % overlap were performed where we randomly initialize the 6 DOF alignment parameters according to a uniform distribution centered at the true alignment and that deviates by  $\pm 45^\circ$  and  $\pm 15$  m in rotation and translation, respectively. The small RMSE values across overlap reflect the effectiveness of our approach and demonstrates its robustness even in cases of small overlap.

### 3.2.3. Ecosystems without trees.

Here, we add a few additional evaluations against co-registration performance in cases where ecosystem does not contain trees. This, with the intention to show the methods' capability to exploit not only structural similarities between objects above ground surface but also from the surface topography itself. The structure in these datasets is

Table 2: Registration RMSE versus % overlap.

Overlap	Orientation (Degrees)			Position (meters)		
	$\theta_{roll}$	$\theta_{pitch}$	$\theta_{yaw}$	$t_x$	$t_y$	$t_z$
~28 %	0.039	0.036	0.034	0.013	0.019	0.011
~ 15%	0.029	0.038	0.032	0.015	0.014	0.015
~ 5%	0.037	0.036	0.045	0.010	0.015	0.013
~ 1%	0.038	0.053	0.051	0.011	0.018	0.011

in this case from the Paramos high-elevation grasslands in Ecuador. Fig.7 shows a representative example with pairs of point clouds each color coded uniformly with  $\approx 5\%$  overlap and with 0.0145 m inlier RMSE. Note that the method is effective in aligning point clouds exploiting only features from topography in as long as there is information in the scene constraining all degrees of freedom in 3D.

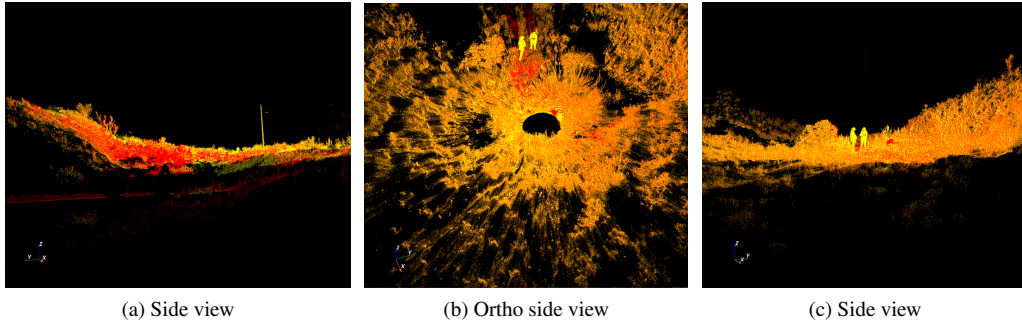


Figure 7: Co-registration in ecosystems without trees. Source scan is color coded yellow while target scan is red.

### 3.3. pre-TLS to post-TLS fire treatment effects registration

Evaluations in this case test the capabilities of pair-wise co-registration in forest ecosystems that underwent changes by the effects of low-intensity fires targeting the ground surface. The scene before and after fire treatments are referred to as the pre and post treatment point clouds, respectively. The severity of the fire was low and the effects produced were qualitatively observable with morphologically thinning changes in the structure of surface fuels (e.g., grass, bushes). These pre and post fire scans were from a prescribed burn at Ft. Stewart Army Base in southeastern Georgia, USA. For reference, we have included in Fig.8(a-b) RGB photos of pre/post treatment effects. Results of LiDAR co-registration were included in Fig.8(c-f) where we see effective alignment of point clouds under the given fire treatment effects. The pre treatment point cloud is color coded yellow while post is red. The resulting overall inlier RMSE was in this case of 0.014 m. Accurate alignment methods for point clouds experiencing pre/post fire or rather in the presence of scene changes in general, can be of high value to science and forest managers. They enable analysis of treatment effects over time and at high resolution spatial scales; a much needed tool for better understanding prescribed fire behavior and which can ultimately lead to improved burn plans.

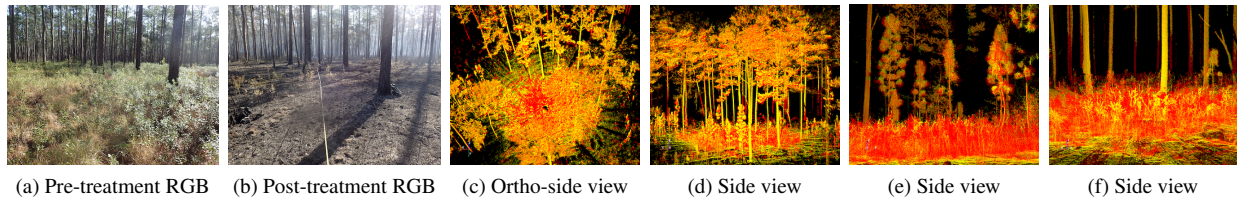


Figure 8: Pre/post treatment effects.

### 3.3.1. Benchmark Evaluations.

Here, we compare the performance of our pair-wise registration against a target-based method benchmark using Styrofoam spheres. In this comparison, the TLS scans from the dataset in [56] were co-registered using our approach and compared against the target-based method for which registration parameters were already available and ground truthed in the referenced dataset. This dataset contains scans of 17 plots, each with 4 scans per plot placed in a triangular pattern (one in the center and the remaining three at each corner 15 m apart from the center) and 9 targets manually placed within the scene. Note that this target-based method results in alignments implicitly validated as ground truth. In Table 3, we summarize the RMSE for all pairs of scans relative to its center scan for all plots. Note that RMSE is computed relative to the registration parameters of the target-based method. From Table 3 we

Table 3: Registration RMSE relative to benchmark target-based method

Orientation (Degrees)			Position (meters)		
$\theta_{\text{roll}}$	$\theta_{\text{pitch}}$	$\theta_{\text{yaw}}$	$t_x$	$t_y$	$t_z$
0.058	0.065	0.032	0.016	0.012	0.007

find that our proposed framework is able to attain the accuracies of target-based methods that often yield close to perfect performance. This validates that our proposed method performs as good as target-based methods without the drawback of any manually placed target requirements nor detection of semantic objects in the scene while also having fully automatic capabilities.

Additional experiments were conducted comparing the performance of co-registration methods alternating between minimizing a similarity function and finding correspondences between LiDAR point returns instead of human engineered or learned features suitable to urban scenarios. As these methods do not rely on lines, contours, planes, normals, edges typical to urban scenarios we deemed them more relevant to the problem at hand. The methods we compared against are the standard iterative closest point [20], coherent point drift [57], gaussian mixture models [58], support vector registration [59] and the more recent trees of gaussian mixtures [60], filterReg [61] and Bayesian coherent point drift [62]. All of these approaches have been implemented and available in the Proreg Python package [63]. For this comparison, twenty pairs of point clouds were selected at random from the available Forest plots and tested each pair for 100 trials with random initializations from the true co-registration parameters deviating by 30 degrees and 15m at one standard deviation. RMSE relative to the six degrees of freedom was then computed and summarized in table 4. Table 4 demonstrates the superiority of our method in registering scenes from heterogeneous Forest scenes

Table 4: Methods comparison of co-Registration performance by RMSE

Approach	Orientation (Degrees)			Position (meters)		
	$\theta_{\text{roll}}$	$\theta_{\text{pitch}}$	$\theta_{\text{yaw}}$	$t_x$	$t_y$	$t_z$
icp [20]	2.324	0.627	25.488	0.88	10.104	0.979
cpd [57]	0.0374	5.3638	29.8273	4.5839	10.0638	0.7630
gmm [58]	0.136	0.0398	18.311	4.583	10.063	0.763
svr [59]	1.724	3.781	23.909	5.388	9.166	0.478
gmmtree [60]	1.590	3.952	28.412	4.6770	8.501	0.618
filterReg [61]	0.512	6.764	30.691	4.451	12.503	0.903
bcpd [62]	0.2248	5.062	21.402	3.2667	12.6039	2.4279
ours	0.0224	0.0002	0.0059	0.0156	0.0149	0.0180

to the compared methods. This Table also, shows that some of the standard methods in the literature have issues in automatically registering scans from complex heterogeneous forests.

### 3.4. Multi-view TLS registration refinement

In multi-view registration, multiple scans viewing the scene from different perspectives are registered in a consistent common coordinate system. In our experiments, we typically choose the center most scan within a forest

inventory plot as the reference common coordinate system, as it has the greatest domain commonality. The single scans in each of the quadrants are first registered in a pair-wise manner relative to the center scan and using the proposed multi-structural level approach. Projection of the aligned scans into the coordinate system of the center scan results in a stitched/accumulated set of scans that were subsequently refined using the proposed bundle refinement approach described in Section 2.2. We find experimentally, that using the paths for each scan  $i$   $\mathbf{c}_i \rightarrow \mathbf{c}_0 \rightarrow \mathbf{c}_j \forall j \notin \{i, 0\}$  and the path in the outer loop of  $\mathbf{c}_0$  without its inclusion (e.g., for  $i = 1$  the path  $\mathbf{c}_1 \rightarrow \mathbf{c}_2 \rightarrow \mathbf{c}_4 \rightarrow \mathbf{c}_3$  in Figure 3) is sufficient for the simultaneous refinement of all the scans within a forest inventory plot. This amounts to a total of 4 paths per scan  $\mathbf{c}_i$  when 5 scans are collected for each inventory plot. Figure 9 is an example that shows views of five aligned scans of a plot with each scan color coded differently. Note that there is a consistent transition between the points of aligned scans throughout the entire scene.

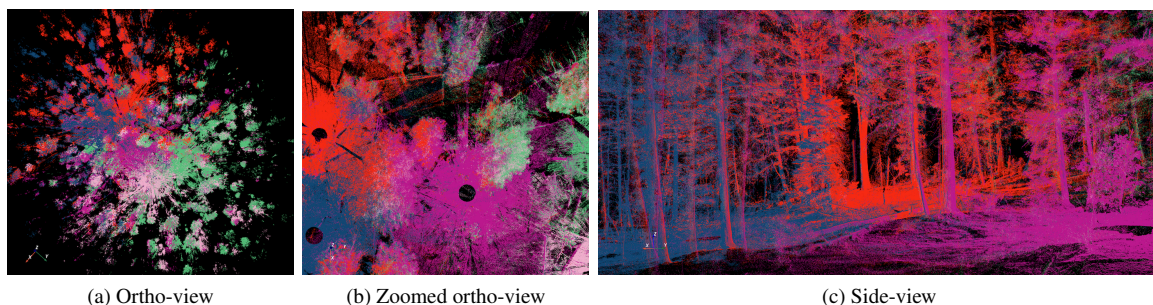


Figure 9: Multi-view alignment of TLS based point clouds

Quantitative performance of our refinement procedure was tested by comparing the point RMSE overall scans in a plot with and without the refinement procedure (only using multi-level registration). A total of 10 plots were tested and the point RMSE is used as the metric of performance. Here, point RMSE is computed over points in the source having at least a correspondence point in the target scan not exceeding 25 cms. Subsequently, a search over the set of corresponding points is performed and the closest target-to-source is chosen. Table 5 summarizes the results. Note that the point RMSE with the additional refinement step gets smaller, thus providing evidence that cycle consistency constraints can improve registration results in forestry multi-view TLS.

Table 5: Point RMSE refinement comparison

Without refinement	With refinement
0.087 (m)	0.0545 (m)

### 3.5. TLS to ALS registration

Validation of our pair-wise multi-level approach was also performed on TLS and ALS registration. In this case, we used the refined set of stitched/accumulated multi-view scans from TLS within an inventory plot along with a cropped to 50x50 m point cloud from ALS centered at the (approximate) GPS location of the center TLS scan (used only for ALS region cropping). A total of 10 TLS plots were registered against ALS where the 6 DOF for alignment were randomly initialized following a random uniform distribution centered at the GPS position of the center scan and deviating by  $\pm 15\text{m}$  and  $\pm 45^\circ$  in the translation and rotation parameters, respectively. A representative example is shown in Fig. 10. The point cloud color coded in red corresponds to the cropped ALS scan while that in green is from the refined multi-view TLS. Note, although both point clouds are captured at different spatial resolution scales with ALS seemingly sparser, but with full overlap, that our approach seems to align both point clouds effectively. Quantitative performance in this case is measured using registration RMSE relative to the RTX in ALS orientation as ground truth similar to as in 3.1 (Note that target based ground truthing is impractical in TLS and ALS co-registration). The RMSE values shows our proposed approach is capable of registering within small errors of ground truth. Note in this case that errors are slightly larger compared to those of only multi-view registration. Main sources we attribute these is the lower resolution of ALS at 10 pts/m<sup>2</sup> compared to that of TLS.

Table 6: TLS to ALS registration RMSE

Orientation (Degrees)			Position (meters)		
$\theta_{\text{roll}}$	$\theta_{\text{pitch}}$	$\theta_{\text{yaw}}$	$t_x$	$t_y$	$t_z$
0.57	0.63	0.26	0.06	0.04	0.03

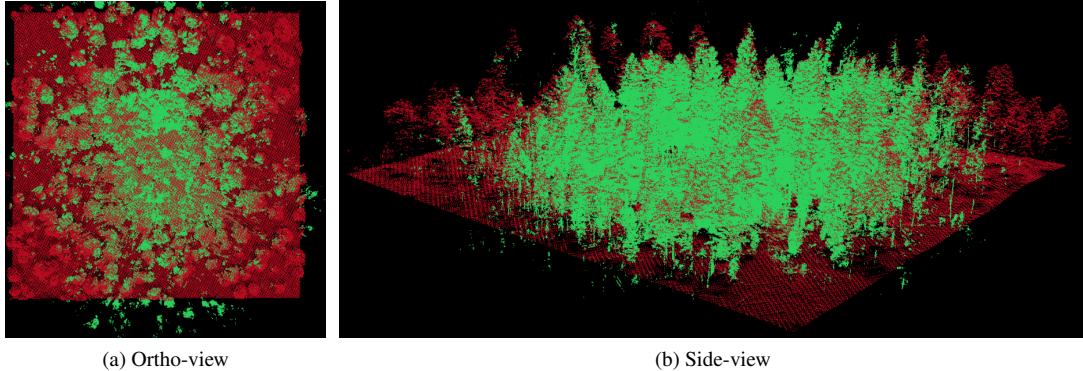


Figure 10: TLS (green) to ALS (red) alignment.

#### 4. Discussion

ALS scan integration technology has long matured thanks to the development of highly reliable RTK position measurement technologies with pose errors below a couple of centimeters in unoccluded areas [64], a characteristic fully satisfied at high aerial elevations. Such RTK measurements allow direct integration of ALS scans into a single consistent large scale source without additional computational processing burden. TLS integration on the other hand, is limited as GPS measurements tend to higher uncertainties in areas of poor or nonexistent satellite based georeferencing, which is typical in natural Forest ecosystems. Methods of TLS integration have heavily relied on manually placed targets in the scene or on semantic scene characterizations to establish semantic relationships between scans for pose corrections. From a practical and reliability standpoint these methods are not efficient nor effective for integrating multi-view TLS and ALS scans at scale. Our novel co-registration approach proposed here bridges this practical and reliable efficiency gap. It was demonstrated here to outperform standard methods [20, 57, 61] in natural ecosystems and to be robust to resolution scales, view-points, scan area overlap, vegetation heterogeneity, topography variations including steep gradient slopes and to ecosystem changes induced by pre/post low-intensity fire effects. It is also fully automatic, capable of self-correcting in cases of noisy GPS measurements and does not require any manually placed targets [12] impractical for ALS + TLS co-registration at scale while performing at the same levels of accuracy.

Altogether, such innovation enables the capability to produce integrated LiDAR maps automatically with the attractive flexibility of access to broad low-res ALS data to rapidly query ecosystem attribute estimation summaries and at the same time access to detailed co-registered high-resolution in-situ understory TLS data for more detailed refined inference of characterizations at the available sites. This flexibility offers the potential to exploit and demonstrate the advantages of either individual or integrated LiDAR sensing sources for ecosystem analysis while also opens up avenues to define the necessary conditions and best strategies for more efficient sensing in ecosystem monitoring. Recent work by [65, 66, 67] has demonstrated the efficiency and efficacy of ecosystem monitoring using single scan in-situ TLS. The technological advances of such models include new capabilities for rapidly extracting highly detailed quantifiable predictions of vegetation attributes and treatment effects in near surface, mid- and general understory composition. However, these models have only been deployed across spatial domains of a few tens of meters in radius. Our innovation here integrating multiple TLS sources and ALS and their synergistic use has the ability to scale in-situ TLS findings as in [65] to deployments over larger area extents.

In summary, our co-registration approach is an enabling technology for large scale ecosystem monitoring through more advanced computational tools of data source integration while also offering new possibilities to more advanced

analysis at scale. It also enables the ability to monitor sites with a more efficient framework to update ecosystem information (as in the pre/post Rx fire co-registration) and with this, the capability to track localized and changes over time. We think our co-registration methodology can also help in establishing trade-offs between ALS, TLS and integrated ALS+TLS based monitoring comparisons and relative to standard forest plot surveying. This, measured through comparisons by time efficiency, human labor requirements, associated costs, performance accuracy, scalability. In future work, we intend to explore a comprehensive investigation if these tradeoffs through the aforementioned metrics. These capabilities altogether can overall improve planning, management and more efficient decision-making of natural ecosystem lands. For example by providing quick and cheap characterizations or forest structure essential for wildlife habitat protection and prescribed burn planning applications.

## 5. Conclusion

In this work, we proposed an automatic targetless multi-level approach to register pair-wise multi-view TLS LiDAR scans and ALS scans to a common reference coordinate system in complex heterogeneous forests. The resulting alignments were further refined using a bundle refinement procedure which promotes cycle consistency between the point clouds to further refine their alignments into a consistent global coordinate system. The qualitative and quantitative results of our experimentation validate that the proposed approach is both efficient and effective in aligning LiDAR scans in forestry at performances comparable with target based methods. It, in addition, showed to be robust in a variety of cases including a diverse set of resolution scales, view-points, overlap, forest heterogeneity (e.g., shrubs below the canopy, different size trees, steepness of the ground surface), low-intensity fire effects and random alignment initializations.

## Acknowledgement

Research presented in this article was supported by the Laboratory Directed Research and Development program of Los Alamos National Laboratory under project number 20220024DR. We thank the United States Department of Agriculture (USDA) Forest Service, Southern Research Station for their support. This research was funded in part by the Department of Defense, Strategic Environmental and Research Development Program, grants number RC19-1119 and RC20-1346, and Department of Defense, Environmental Security Technology Certification Program, grant number RC20-7189. This research was also funded in part by the USDA Center for International Programs and U.S. Agency for International Development. The findings and conclusions in this publication are those of the authors and should not be construed to represent any official USDA or U.S. Government determination or policy.

## References

### References

- [1] U. FAO, The state of the world's forests 2020, in: Forests, biodiversity and people, Rome, Italy, 2020, p. 214. doi:<https://doi.org/10.4060/ca8642en>.
- [2] J. C. White, N. C. Coops, M. A. Wulder, M. Vastaranta, T. Hilker, P. Tompalski, Remote sensing technologies for enhancing forest inventories: A review, *Canadian Journal of Remote Sensing* 42 (5) (2016) 619–641.
- [3] A. Atchley, J. A. Linn, Rodman, C. Hoffman, J. D. Hyman, F. Pimont, C. Sieg, R. S. Middleton, Effects of fuel spatial distribution on wildland fire behaviour, *International Journal of Wildland Fire* 30 (3) (2021) 179–189.
- [4] E. Tomppo, T. Gschwantner, M. Lawrence, R. E. McRoberts, K. Gabler, K. Schadauer, C. Vidal, A. Lanz, G. Ståhl, E. Cienciala, National forest inventories, Pathways for Common Reporting, *European Science Foundation* 1 (2010) 541–553.
- [5] R. O. Dubayah, J. B. Drake, Lidar remote sensing for forestry, *Journal of forestry* 98 (6) (2000) 44–46.
- [6] J. Hyypä, X. Yu, H. Hyypä, M. Vastaranta, M. Holopainen, A. Kukko, H. Kaartinen, A. Jaakkola, M. Vaaja, J. Koskinen, et al., Advances in forest inventory using airborne laser scanning, *Remote sensing* 4 (5) (2012) 1190–1207.
- [7] T. Hilker, M. van Leeuwen, N. C. Coops, M. A. Wulder, G. J. Newnham, D. L. Jupp, D. S. Culvenor, Comparing canopy metrics derived from terrestrial and airborne laser scanning in a douglas-fir dominated forest stand, *Trees* 24 (5) (2010) 819–832.
- [8] M. Holopainen, V. Kankare, M. Vastaranta, X. Liang, Y. Lin, M. Vaaja, X. Yu, J. Hyypä, H. Hyypä, H. Kaartinen, et al., Tree mapping using airborne, terrestrial and mobile laser scanning—a case study in a heterogeneous urban forest, *Urban forestry & urban greening* 12 (4) (2013) 546–553.
- [9] T. Hilker, N. C. Coops, D. S. Culvenor, G. Newnham, M. A. Wulder, C. W. Bater, A. Siggins, A simple technique for co-registration of terrestrial lidar observations for forestry applications, *Remote sensing letters* 3 (3) (2012) 239–247.

- [10] V. Kankare, J. Vauhkonen, T. Tanhuanpää, M. Holopainen, M. Vastaranta, M. Joensuu, A. Krooks, J. Hyypää, H. Hyypää, P. Alho, et al., Accuracy in estimation of timber assortments and stem distribution—a comparison of airborne and terrestrial laser scanning techniques, *ISPRS Journal of Photogrammetry and Remote Sensing* 97 (2014) 89–97.
- [11] S. Bauwens, H. Bartholomeus, K. Calders, P. Lejeune, Forest inventory with terrestrial lidar: A comparison of static and hand-held mobile laser scanning, *Forests* 7 (6) (2016) 127.
- [12] X. Ge, Q. Zhu, Target-based automated matching of multiple terrestrial laser scans for complex forest scenes, *ISPRS Journal of Photogrammetry and Remote Sensing* 179 (2021) 1–13.
- [13] A. Bienert, H.-G. Maas, Methods for the automatic geometric registration of terrestrial laser scanner point clouds in forest stands, in: *Proceedings of the ISPRS Workshop on Laser Scanning, Societe Francaise de Photogrammetrie et de Teledetection Lemmer, 2009*, pp. 1–2.
- [14] D. Kelbe, J. Van Aardt, P. Romanczyk, M. Van Leeuwen, K. Cawse-Nicholson, Marker-free registration of forest terrestrial laser scanner data pairs with embedded confidence metrics, *IEEE transactions on geoscience and remote sensing* 54 (7) (2016) 4314–4330.
- [15] J. Liu, X. Liang, J. Hyypää, X. Yu, M. Lehtomäki, J. Pyörälä, L. Zhu, Y. Wang, R. Chen, Automated matching of multiple terrestrial laser scans for stem mapping without the use of artificial references, *International Journal of Applied Earth Observation and Geoinformation* 56 (2017) 13–23.
- [16] J.-F. Tremblay, M. Béland, Towards operational marker-free registration of terrestrial lidar data in forests, *ISPRS Journal of Photogrammetry and Remote Sensing* 146 (2018) 430–435.
- [17] P. Polewski, W. Yao, L. Cao, S. Gao, Marker-free coregistration of uav and backpack lidar point clouds in forested areas, *ISPRS Journal of Photogrammetry and Remote Sensing* 147 (2019) 307–318.
- [18] X. Ge, Q. Zhu, L. Huang, S. Li, S. Li, Global registration of multiview unordered forest point clouds guided by common subgraphs, *IEEE Transactions on Geoscience and Remote Sensing* 60 (2021) 1–14.
- [19] X. Liang, A. Kukko, H. Kaartinen, J. Hyypää, X. Yu, A. Jaakkola, Y. Wang, Possibilities of a personal laser scanning system for forest mapping and ecosystem services, *Sensors* 14 (1) (2014) 1228–1248.
- [20] P. J. Besl, N. D. McKay, A method for registration of 3-d shapes, *IEEE Transactions on Pattern Analysis and Machine Intelligence* 14 (2) (1992) 239–256. doi:10.1109/34.121791.
- [21] Y. Chen, G. Medioni, Object modelling by registration of multiple range images, *Image and vision computing* 10 (3) (1992) 145–155.
- [22] D. Aiger, N. J. Mitra, D. Cohen-Or, 4pointss congruent sets for robust pairwise surface registration, *ACM Trans. Graph.* 27 (3) (2008) 85:1–85:10. doi:10.1145/1360612.1360684. URL <http://doi.acm.org/10.1145/1360612.1360684>
- [23] R. B. Rusu, N. Blodow, M. Beetz, Fast point feature histograms (fpfh) for 3d registration, in: *2009 IEEE International Conference on Robotics and Automation*, 2009, pp. 3212–3217. doi:10.1109/ROBOT.2009.5152473.
- [24] Y. Li, G. Wang, X. Ji, Y. Xiang, D. Fox, Deepim: Deep iterative matching for 6d pose estimation, in: *Proceedings of the European Conference on Computer Vision (ECCV)*, 2018, pp. 683–698.
- [25] W. Lu, G. Wan, Y. Zhou, X. Fu, P. Yuan, S. Song, Deepvcp: An end-to-end deep neural network for point cloud registration, in: *Proceedings of the IEEE/CVF International Conference on Computer Vision*, 2019, pp. 12–21.
- [26] Z. Dong, F. Liang, B. Yang, Y. Xu, Y. Zang, J. Li, Y. Wang, W. Dai, H. Fan, J. Hyypää, et al., Registration of large-scale terrestrial laser scanner point clouds: A review and benchmark, *ISPRS Journal of Photogrammetry and Remote Sensing* 163 (2020) 327–342.
- [27] C. Brenner, C. Dold, N. Ripperda, Coarse orientation of terrestrial laser scans in urban environments, *ISPRS journal of photogrammetry and remote sensing* 63 (1) (2008) 4–18.
- [28] T. Sumi, S. Kanai, et al., Multiple tfs point cloud registration based on point projection images., *International Archives of the Photogrammetry, Remote Sensing & Spatial Information Sciences* 42 (2).
- [29] B. Xiong, D. Li, Z. Zhou, F. Li, Fast registration of terrestrial lidar point clouds based on gaussian-weighting projected image matching, *Remote Sensing* 14 (6) (2022) 1466.
- [30] X. Xu, P. Wang, X. Gan, J. Sun, Y. Li, L. Zhang, Q. Zhang, M. Zhou, Y. Zhao, X. Li, Automatic marker-free registration of single tree point-cloud data based on rotating projection, *Artificial Intelligence in Agriculture* 6 (2022) 176–188.
- [31] H. Guan, Y. Su, X. Sun, G. Xu, W. Li, Q. Ma, X. Wu, J. Wu, L. Liu, Q. Guo, A marker-free method for registering multi-scan terrestrial laser scanning data in forest environments, *ISPRS Journal of Photogrammetry and Remote Sensing* 166 (2020) 82–94.
- [32] W. Dai, B. Yang, X. Liang, Z. Dong, R. Huang, Y. Wang, J. Pyörälä, A. Kukko, Fast registration of forest terrestrial laser scans using key points detected from crowns and stems, *International Journal of Digital Earth* 13 (12) (2020) 1585–1603.
- [33] H. Guan, Y. Su, T. Hu, R. Wang, Q. Ma, Q. Yang, X. Sun, Y. Li, S. Jin, J. Zhang, et al., A novel framework to automatically fuse multiplatform lidar data in forest environments based on tree locations, *IEEE Transactions on Geoscience and Remote Sensing* 58 (3) (2019) 2165–2177.
- [34] M. Kedzierski, A. Fryskowska, Terrestrial and aerial laser scanning data integration using wavelet analysis for the purpose of 3d building modeling, *Sensors* 14 (7) (2014) 12070–12092.
- [35] T.-A. Teo, S.-H. Huang, Surface-based registration of airborne and terrestrial mobile lidar point clouds, *Remote Sensing* 6 (12) (2014) 12686–12707.
- [36] H. Wu, M. Scaioni, H. Li, N. Li, M. Lu, C. Liu, Feature-constrained registration of building point clouds acquired by terrestrial and airborne laser scanners, *Journal of Applied Remote Sensing* 8 (1) (2014) 083587–083587.
- [37] B. Yang, Y. Zang, Z. Dong, R. Huang, An automated method to register airborne and terrestrial laser scanning point clouds, *ISPRS Journal of Photogrammetry and Remote Sensing* 109 (2015) 62–76.
- [38] X. Cheng, X. Cheng, Q. Li, L. Ma, Automatic registration of terrestrial and airborne point clouds using building outline features, *IEEE Journal of Selected Topics in Applied Earth Observations and Remote Sensing* 11 (2) (2018) 628–638.
- [39] X. Ling, R. Qin, A graph-matching approach for cross-view registration of over-view and street-view based point clouds, *ISPRS Journal of Photogrammetry and Remote Sensing* 185 (2022) 2–15.
- [40] X. Wang, Z. Yang, X. Cheng, J. Stoter, W. Xu, Z. Wu, L. Nan, Efficient registration of forest point clouds by global matching of relative stem positions, *arXiv preprint arXiv:2112.11121*.
- [41] M. Hauglin, V. Lien, E. Næsset, T. Gobakken, Geo-referencing forest field plots by co-registration of terrestrial and airborne laser scanning

- data, *International journal of remote sensing* 35 (9) (2014) 3135–3149.
- [42] C. Paris, D. Kelbe, J. Van Aardt, L. Bruzzone, A novel automatic method for the fusion of als and tls lidar data for robust assessment of tree crown structure, *IEEE Transactions on Geoscience and Remote Sensing* 55 (7) (2017) 3679–3693.
- [43] W. Dai, B. Yang, X. Liang, Z. Dong, R. Huang, Y. Wang, W. Li, Automated fusion of forest airborne and terrestrial point clouds through canopy density analysis, *ISPRS Journal of Photogrammetry and Remote Sensing* 156 (2019) 94–107.
- [44] Q. Liu, J. Wang, W. Ma, J. Zhang, Y. Deng, D. Shao, D. Xu, Y. Liu, Target-free uls-tls point-cloud registration for alpine forest lands, *Computers and Electronics in Agriculture* 190 (2021) 106460.
- [45] C. E. Shannon, A mathematical theory of communication, *The Bell system technical journal* 27 (3) (1948) 379–423.
- [46] G. Pandey, J. R. McBride, S. Savarese, R. M. Eustice, Automatic targetless extrinsic calibration of a 3d lidar and camera by maximizing mutual information, in: *Twenty-Sixth AAAI Conference on Artificial Intelligence*, 2012.
- [47] J. Castorena, C. Creusere, D. Voelz, Using finite moment rate of innovation for lidar waveform complexity estimation, in: *2010 Conference Record of the Forty Fourth Asilomar Conference on Signals, Systems and Computers*, IEEE, 2010, pp. 608–612.
- [48] J. Castorena, C. D. Creusere, D. Voelz, Modeling lidar scene sparsity using compressive sensing, in: *2010 IEEE International Geoscience and Remote Sensing Symposium*, IEEE, 2010, pp. 2186–2189.
- [49] J. A. Hartigan, M. A. Wong, Algorithm as 136: A k-means clustering algorithm, *Journal of the royal statistical society. series c (applied statistics)* 28 (1) (1979) 100–108.
- [50] M. A. Fischler, R. C. Bolles, Random sample consensus: a paradigm for model fitting with applications to image analysis and automated cartography, *Communications of the ACM* 24 (6) (1981) 381–395.
- [51] J. Castorena, G. V. Puskorius, G. Pandey, Motion guided lidar-camera self-calibration and accelerated depth upsampling for autonomous vehicles, *Journal of Intelligent & Robotic Systems* 100 (3) (2020) 1129–1138.
- [52] D. P. Bertsekas, The auction algorithm: A distributed relaxation method for the assignment problem, *Annals of operations research* 14 (1) (1988) 105–123.
- [53] M. Moakher, Means and averaging in the group of rotations, *SIAM Journal on Matrix Analysis and Applications* 24(1) (2002) 597 – 621.
- [54] R. Hartley, K. Aftab, J. Trunpf, L1 rotation averaging using the weiszfeld algorithm, in: *CVPR 2011*, 2011, pp. 3041–3048. doi:10.1109/CVPR.2011.5995745.
- [55] Q.-Y. Zhou, J. Park, V. Koltun, Open3D: A modern library for 3D data processing, arXiv:1801.09847.
- [56] C. Gollob, T. Ritter, A. Nothdurft, Comparison of 3d point clouds obtained by terrestrial laser scanning and personal laser scanning on forest inventory sample plots, *Data* 5 (4) (2020) 103.
- [57] A. Myronenko, X. Song, Point set registration: Coherent point drift, *IEEE transactions on pattern analysis and machine intelligence* 32 (12) (2010) 2262–2275.
- [58] B. Jian, B. C. Vemuri, Robust point set registration using gaussian mixture models, *IEEE transactions on pattern analysis and machine intelligence* 33 (8) (2010) 1633–1645.
- [59] D. Campbell, L. Petersson, An adaptive data representation for robust point-set registration and merging, in: *Proceedings of the IEEE international conference on computer vision*, 2015, pp. 4292–4300.
- [60] B. Eckart, K. Kim, J. Kautz, Fast and accurate point cloud registration using trees of gaussian mixtures, arXiv preprint arXiv:1807.02587.
- [61] W. Gao, R. Tedrake, Filterreg: Robust and efficient probabilistic point-set registration using gaussian filter and twist parameterization, in: *Proceedings of the IEEE/CVF Conference on Computer Vision and Pattern Recognition*, 2019, pp. 11095–11104.
- [62] O. Hirose, A bayesian formulation of coherent point drift, *IEEE transactions on pattern analysis and machine intelligence* 43 (7) (2020) 2269–2286.
- [63] Kenta-Tanaka et al., probreg.  
URL <https://probreg.readthedocs.io/en/latest/>
- [64] C. Rizos, et al., Network rtk research and implementation-a geodetic perspecti, *Positioning* 1 (02).
- [65] S. Pokswinski, M. R. Gallagher, N. S. Skowronski, E. L. Loudermilk, C. Hawley, D. Wallace, A. Everland, J. Wallace, J. K. Hiers, A simplified and affordable approach to forest monitoring using single terrestrial laser scans and transect sampling, *MethodsX* 8 (2021) 101484.
- [66] C. Anderson, S. Dietz, S. Pokswinski, A. Jenkins, M. Kaeser, J. Hiers, B. Pelc, Traditional field metrics and terrestrial lidar predict plant richness in southern pine forests, *Forest Ecology and Management* 491 (2021) 119118.
- [67] E. L. Loudermilk, S. Pokswinski, C. M. Hawley, A. Maxwell, M. R. Gallagher, N. S. Skowronski, A. T. Hudak, C. Hoffman, J. K. Hiers, Terrestrial laser scan metrics predict surface vegetation biomass and consumption in a frequently burned southeastern us ecosystem, *bioRxiv* (2023) 2023–01.